Imperial College London

A phenomenological model for modified gravitational wave dispersion relations

Submitted by Michelle Gurevich
Supervised by Prof. Carlo Contaldi

June 2022

A thesis submitted in partial fulfilment of the requirements for the degree of MSc in Physics with Extended Research and the Diploma of Imperial College London.

Abstract

Gravitational wave measurements from LIGO have previously been used to place effective constraints on Lorentz-violating quantities such as the massive graviton. We expect an influx of detections in the $10^{-1} - 10^{-4}$ Hz frequency range once LISA is operational, allowing such constraints to be generated for gravitational waves transversing multiple frequency bands. This will open up gravitational wave astronomy to an exciting multi-messenger era and allow theories of modified gravity to be rigorously tested. We develop a phenomenological model to study the frequency-dependent effects of modifications to gravitational wave dispersion relations, in the hopes of constraining data for an effective field theory of gravity. This model is sufficiently general to allow for the choice of phenomenological parameters to be updated as needed. A Fisher analysis is performed to constrain results in parameter space. Though the model is developed for LIGO and LISA, extensions to the Einstein Telescope are discussed.

Acknowledgements

I would like to thank my supervisor, Carlo, for introducing me to the many exciting applications of gravitational waves; Mauro, for helping to better understand some of these; Sebastian and Linus, for their help in refining and proofreading.

When I began this research, I knew only that I was eager to study gravitational waves after learning about them in a general relativity course. Carlo agreed to take me on as a student, and his guidance this past year inspired me immensely. My plans to continue in theoretical physics are due in no small part to his patience and support, and I am grateful to have had a supervisor like him early in my research career.

Finally, a sincere and heartfelt thank you to Thomas – for everything.

This work would not have been possible without the open-source `PyCBC` code written by scientists from the LIGO and Virgo collaborations. Though it was not used in the final phenomenological model, the publicly available `CAMB` code was instrumental to my understanding of the underlying cosmology and distance metrics from a coding perspective. I would like to express my gratitude to all those who develop and maintain these repositories.

Declaration

I declare that the work presented in this thesis is my own and it was wholly done while being a student at Imperial College London. I have acknowledged all my sources, referenced quotations, and credited publicly available code.

Conventions

Partial derivatives are written $\frac{\partial}{\partial x^\mu} = \partial_\mu = {}_{,\mu}$ and covariant derivatives ∇_μ
The metric signature is given by (-1, 1, 1, 1) and the metric $g_{\mu\nu} = \text{diag}(-1, 1, 1, 1)$

List of Abbreviations

BBH - **B**inary **B**lack **H**ole
ET - **E**instein **T**elescope
EMRI - **E**xtreme **M**ass **R**atio **I**nspiral
FRW - **F**riedmann-Lemaitre-**R**obertson-**W**alker
GR -**G**eneral **R**elativity
GW - **G**ravitational **W**ave
IMBH - **I**ntermediate **M**ass **B**lack **H**ole
LIGO - **L**aser **I**nterferometer **G**ravitational-Wave **O**bservatory
LISA - **L**aser **I**nterferometer **S**pace **A**ntenna
PN - **P**ost **N**ewtonian
SNR - **S**ignal to **N**oise **R**atio

Contents

List of Tables

List of Figures

Chapter 1

Introduction

As black holes merge and collide, they produce ripples in spacetime not unlike those from a stone skipped across a pond. These ripples, called gravitational waves, carry information that informs our theories of the origins and evolution of the universe, and the very structure of gravity. We know general relativity is an incomplete description of reality, and a search for violations helps us discover precisely where it breaks down [1]. The high energy scales at which this is expected to happen can be probed to determine constraints on, for example, gravitational wave dispersion relations. These constraints can then be used to formulate an effective field theory framework for gravity – one that we expect would provide a more complete representation of reality.

We begin by considering a binary black hole system in the context of standard general relativity. As the component masses, m_1 and m_2, approach each other, they distort spacetime radially (shown in Fig. (1.1)). In GR, this distortion is described mathematically as waves propagating at the speed of light [2]. The component masses experience an inspiral phase as their orbits grow closer, and eventually they merge into a single, coalesced object of chirp mass,

$$\mathcal{M} = \frac{(m_1 m_2)^{3/5}}{(m_1 + m_2)^{1/5}} = \frac{c^3}{G}\left[\frac{5}{96}\pi^{-8/3} f^{-11/3}\dot{f}\right]^{3/5} \tag{1.1}$$

where f is observed frequency, and G and c the familiar constants as shown in Table 1.1 [3]. The chirp mass is then the effective mass of the system once energy dissipation due to gravitational wave radiation has been accounted for. This is also the quantity, expressed as a multiple of solar masses, which is either within or outside of some known sensitivity band for a particular instrument. This is an important consideration as it drives the

Physical constant	Symbol	Value
Compton wavelength [of electron]	$\lambda_C = h/m_{[e]}c$	$[2.426 \times 10^{-12}\text{m}]$ N m^2 kg^{-2}
Gravitational constant	G	6.6743×10^{-11} N m^2 kg^{-2}
Planck constant	h	6.626×10^{-34} J s
Planck constant, reduced	$\hbar = h/2\pi$	1.055×10^{-34} J s
Speed of light in a vacuum	c	2.998×10^{-8} m s^{-1}

Table 1.1: Table of fundamental physical constants with values taken from [5].

discussion of the kinds of systems our model will address.

We want to probe frequency-dependent modifications to the dispersion relations of gravitational waves. This involves describing the waveform in (an approximation to) standard GR, and introducing modified quantities that drive its propagation over cosmological distances. These are generalized in a model that takes in an unmodified waveform and produces a new, modified waveform. Since the modified waveform should not deviate greatly from the original signal (equivalent to recognising GR is indeed an accurate theory), the modifications introduced are small. More precisely, some are on the order of the Planck scale (see Table 1.1). For this reason, many of the figures consider the ratio of modified to unmodified waveform, or the phenomenological parameter in its limit, so as to track changes to wave propagation. This may prompt the question: if GR is indeed a valid theory of gravitation, why do we introduce modifications at all? And can constraining the effects of these modifications truly provide a more complete understanding?

1.1 General relativity: an incomplete theory

Gravitational waves quantify the energy released by an accelerating object [2], and the resulting distortion of spacetime should be observed to propagate at the speed of light under GR [6]. However, we expect general relativity is a low-energy approximation of an effective field theory (EFT), one that can generalise general relativity rather than dismissing it outright [7]. If there are differences between the predictions of GR and observation, they would necessarily become visible at high energy scales or low length scales. As such, the mergers of black holes or other extremely massive objects are a likely candidate. These differences are described in multiple frameworks of modified gravity, and generally involve a massive graviton that corresponds to a change in the speed of the wave propagation, or gravitational wave dispersion [8][9]. Conversely, the detection of a modified phase in a gravitational wave signal would be compelling evidence that the wave

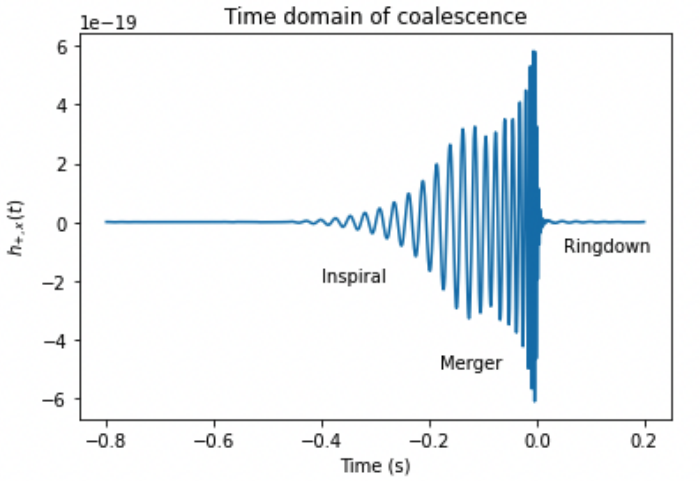

Figure 1.1: TOP: Coalescence of a binary black hole system in the time domain. The two objects orbit each other in increasingly closer proximity, producing gravitational waves of increasingly higher frequency, before coalescing into a single object. BOTTOM: Compare to the evolution of the waveform signal produced by this system and shown on an axis of time before and after the final coalescence. Adapted from [4].

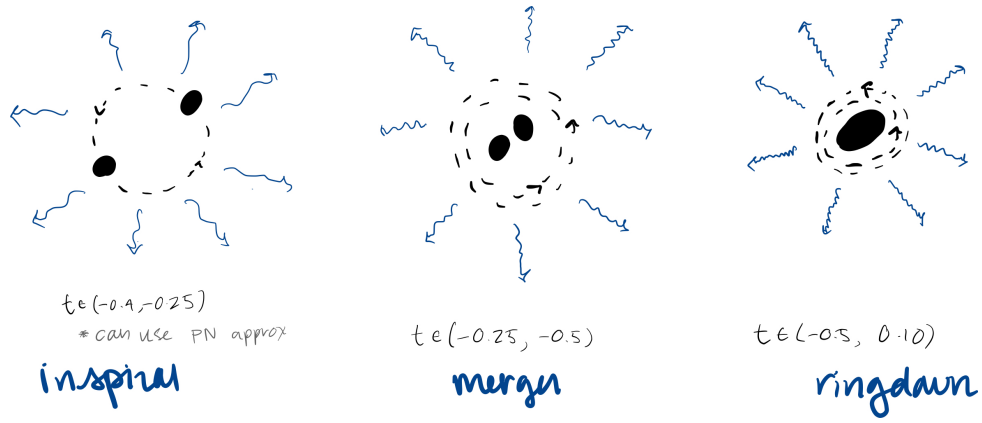

is mediated by some massive graviton. This would have implications for Beyond Standard Model physics [10], quantum gravity [11], and the cosmological constant problem [12].

Determining constraints on a modified signal is one avenue for isolating the possible forms a nonstandard waveform could take and interpreting observed signals. This is important as currently many of the nonstandard waveforms produced by LIGO are dismissed as 'glitches', and it is possible we are missing out on a significant portion of evidence for beyond GR theory [13]. By characterising the modified signal in a rigorous framework and controlling for frequency effects, we hope to provide a tool for approaching nonstandard observables in a systematic, coherent way.

1.2 Data constraints using gravitational waves

It is useful to note there is evidence in the work of [14], [15], and others to motivate this project. In particular, constraints on the speed of propagation of gravitational waves have been determined previously.

For example, binary systems sometimes have electromagnetic counterparts, such as gamma-ray bursts, emitted alongside gravitational waves. These can be used to constrain the speed at which the gravitational waves propagate. This strategy was used for **GW170817**, allowing for better constraints to the upper bound of time to travel to the detector [16], and for **GW150914** to constrain Lorentz violation effects [17]. Such constraints are particularly useful for frequencies that correspond to cutoffs beyond which gravitational waves may travel at different speeds than in lower energy regimes [14]. Crucially, it can be shown that for frequency ranges typical of future detectors it will not be necessary to have an EM counterpart to place similar constraints [16].

The contribution offered here is a systematic way to reproduce some of these constraints using a phenomenological model. The model is built around a sufficiently generic dispersion relation which, depending on the choice of certain parameter values, corresponds to modified theories of gravity.

Chapter 2

Theoretical background

2.1 The weak-field limit of general relativity

Gravitational waves are small tensor perturbations of the metric, $g_{\mu\nu}$, and so it is useful to work in a preferred set of coordinates where the metric assumes the form,

$$g_{\mu\nu} = \eta_{\mu\nu} + h_{\mu\nu} \tag{2.1}$$

with $|h_{\mu\nu}| \ll 1$ and for $\eta_{\mu\nu} = \text{diag}(-1, 1, 1, 1)$ the metric in flat, Minkowski space. We can neglect higher-order terms of $h_{\mu\nu}$ and work to first-order where necessary. We will see that doing so produces a linearized form of the Einstein field equations of general relativity by way of a calculation of the necessary curvature tensors. The introduction of a particular gauge will, in turn, motivate a search for the solution to the resulting wave equation.

Noting that for a linear metric of the form Eq. (2.1) the inverse is simply,

$$g^{\mu\nu} = \eta^{\mu\nu} - h^{\mu\nu} + \mathcal{O}(h^2) \tag{2.2}$$

we can calculate the associated first-order Christoffel symbols using their usual definition and noting that $g_{\mu\nu,\rho} = (\eta_{\mu\nu} + h_{\mu\nu})_{,\rho} = h_{\mu\nu,\rho}$ (where we introduce a simplified notation

for partial derivatives as show in the Notational convention section),

$$\begin{aligned}\Gamma^{\mu}_{\nu\rho} &= \frac{1}{2}g^{\mu\sigma}\left(\partial_{\rho}g_{\sigma\nu} + \partial_{\nu}g_{\sigma\rho} - \partial_{\sigma}g_{\nu\rho}\right) \\ &= \frac{1}{2}\eta^{\mu\sigma}\left(h_{\sigma\nu,\rho} + h_{\sigma\rho,\nu} - h_{\nu\rho,\sigma}\right)\end{aligned} \tag{2.3}$$

We do this to facilitate practical calculations involving the metric connection. In particular, Eq. (2.3) allows us to calculate the Riemann tensor. We do this to first-order, ignoring the higher-order terms resulting from products of Christoffel symbols,

$$\begin{aligned}R^{\mu}_{\nu\rho\sigma} &= \Gamma^{\mu}_{\nu\sigma,\rho} - \Gamma^{\mu}_{\nu\rho,\sigma} + \Gamma^{\mu}_{\rho\alpha}\Gamma^{\alpha}_{\nu\sigma} - \Gamma^{\mu}_{\sigma\alpha}\Gamma^{\alpha}_{\nu\rho} \\ &= \left[\frac{1}{2}\eta^{\mu\alpha}\left(h_{\alpha\nu,\sigma} + h_{\alpha\sigma,\nu} - h_{\nu\sigma,\alpha}\right)\right]_{,\rho} - \left[\frac{1}{2}\eta^{\mu\alpha}\left(h_{\alpha\nu,\rho} + h_{\alpha\rho,\nu} - h_{\nu\rho,\alpha}\right)\right]_{,\sigma} + \mathcal{O}(\Gamma\Gamma) \\ &= \frac{1}{2}\eta^{\mu\alpha}\left(h_{\alpha\nu,\sigma\rho} + h_{\alpha\sigma,\nu\rho} - h_{\nu\sigma,\alpha\rho} - h_{\alpha\nu,\rho\sigma} - h_{\alpha\rho,\nu\sigma} + h_{\nu\rho,\alpha\sigma}\right) + ... \\ &= \frac{1}{2}\eta^{\mu\alpha}\left(h_{\alpha\sigma,\nu\rho} + h_{\nu\rho,\alpha\sigma} - h_{\nu\sigma,\alpha\rho} - h_{\alpha\rho,\nu\sigma}\right) + ...\end{aligned} \tag{2.4}$$

where we have made use of the fact that partial derivatives commute to cancel the first term with the fourth in the last expression. We can lower the μ index of the tensor on the left-hand side by introducing a factor of the metric, and relabelling the indices in the last expression since λ is a free index.

$$\begin{aligned}R_{\mu\nu\rho\sigma} = \eta_{\mu\lambda}R^{\lambda}_{\nu\rho\sigma} &= \eta_{\mu\lambda}\left[\Gamma^{\lambda}_{\nu\sigma,\rho} - \Gamma^{\lambda}_{\nu\rho,\sigma}\right] \\ &= \frac{1}{2}\eta_{\mu\lambda}\eta^{\mu\alpha}\left(h_{\alpha\sigma,\nu\rho} + h_{\nu\rho,\alpha\sigma} - h_{\nu\sigma,\alpha\rho} - h_{\alpha\rho,\nu\sigma}\right) \\ &= \frac{1}{2}\delta^{\alpha}_{\lambda}\left(h_{\alpha\sigma,\nu\rho} + h_{\nu\rho,\alpha\sigma} - h_{\nu\sigma,\alpha\rho} - h_{\alpha\rho,\nu\sigma}\right) \\ &= \frac{1}{2}\left(h_{\lambda\sigma,\nu\rho} + h_{\nu\rho,\lambda\sigma} - h_{\nu\sigma,\lambda\rho} - h_{\lambda\rho,\nu\sigma}\right) \\ &= \frac{1}{2}\left(h_{\mu\sigma,\nu\rho} + h_{\nu\rho,\mu\sigma} - h_{\nu\sigma,\mu\rho} - h_{\mu\rho,\nu\sigma}\right)\end{aligned} \tag{2.5}$$

The resulting form of the Riemann tensor $R_{\mu\nu\rho\sigma} = \frac{1}{2}\left(h_{\mu\sigma,\nu\rho} + h_{\nu\rho,\mu\sigma} - h_{\nu\sigma,\mu\rho} - h_{\mu\rho,\nu\sigma}\right)$ derived in Eq. (2.5) is more convenient because it allows us to compute the Ricci tensor simply.

We introduce factor of $\eta^{\mu\rho}$ to this tensor equation,

$$\begin{aligned} R_{\nu\sigma} = \eta^{\mu\rho} R_{\mu\nu\rho\sigma} &= \frac{1}{2}\left(\eta^{\mu\rho} h_{\mu\sigma,\nu\rho} + \eta^{\mu\rho} h_{\nu\rho,\mu\sigma} - \eta^{\mu\rho} h_{\mu\rho,\nu\sigma} - \eta^{\mu\rho} h_{\nu\sigma,\mu\rho}\right) \\ &= \frac{1}{2}\left(h^{\rho}_{\sigma,\nu\rho} + h^{\mu}_{\nu,\mu\sigma} - h_{,\nu\sigma} - \Box h_{\nu\sigma}\right) \\ &= \frac{1}{2}\left(h^{\mu}_{\sigma,\nu\mu} + h^{\mu}_{\nu,\mu\sigma} - h_{,\sigma\nu} - \Box h_{\nu\sigma}\right) \end{aligned} \tag{2.6}$$

where the d'Alembert operator is defined by $\Box = \partial^{\alpha}\partial_{\alpha} = -\partial_t^2 + \nabla^2$ for $c = 1$. The Ricci curvature tensor is determined by the choice of metric and can be thought of as a measure of how closely the spacetime locally approximates flat (Minkowski) spacetime, for which it is identically zero [18]. It also allows us to compute the Einstein tensor and to finish deriving the linearized Einstein field equations, which govern the relationship between energy and curvature in general relativity.

To proceed, we define the metric perturbation term $h \equiv \eta^{\mu\nu} h_{\mu\nu}$ through a contraction along its two indices, and contract Eq. (2.6) along $\eta^{\nu\sigma}$ to find the Ricci scalar,

$$\begin{aligned} R = \eta^{\nu\sigma} R_{\nu\sigma} &= \frac{1}{2}\left(\eta^{\nu\sigma} h^{\mu}_{\sigma,\nu\mu} + \eta^{\nu\sigma} h^{\mu}_{\nu,\mu\sigma} - \eta^{\nu\sigma}\Box h_{,\sigma\nu} - \eta^{\nu\sigma}\Box h_{\nu\sigma}\right) \\ &= \frac{1}{2}\left(h^{\mu}_{,\mu} + h^{\mu}_{,\mu} - 2\Box h\right) \\ &= h^{\mu\nu}{}_{,\mu\nu} - \Box h \end{aligned} \tag{2.7}$$

Combining Eq. (2.6) and Eq. (2.7) gives the Einstein tensor,

$$\begin{aligned} G_{\mu\nu} = R_{\mu\nu} - \frac{1}{2}\eta_{\mu\nu} R &= \frac{1}{2}\left(h^{\rho}_{\mu,\rho\nu} + h^{\rho}_{\nu,\rho\mu} - h_{,\mu\nu} - \Box h_{\mu\nu}\right) - \frac{1}{2}\eta_{\mu\nu}\left(h^{\rho\sigma}_{,\rho\sigma} - \Box h\right) + \mathcal{O}\left(h^2\right) \\ &= \frac{1}{2}\left(h^{\rho}_{\mu,\rho\nu} + h^{\rho}_{\nu,\rho\mu} - h_{,\mu\nu} - \Box h_{\mu\nu} - \eta_{\mu\nu} h^{\rho\sigma}_{,\rho\sigma} + \eta_{\mu\nu}\Box h\right) + \mathcal{O}\left(h^2\right) \end{aligned} \tag{2.8}$$

We can use the Bianchi identity, which states that if the partial derivatives of a tensor at a point equal the covariant derivatives at that point, then the partials of the Riemann tensors sum to zero. In the linearized case of Eq. (2.8), since $\partial_{\mu} G^{\mu\nu} = 0$, we have $\nabla_{\mu} G^{\mu\nu} = 0$ and the condition is satisfied. Thus since [18],

$$R_{\mu\nu} - \frac{1}{2}\eta_{\mu\nu} R = 8\pi G T_{\mu v} \tag{2.9}$$

by keeping only those terms of the stress-energy tensor $T_{\mu\nu}$ that are linear in $h_{\rho\sigma}$, we can

write the linearized Einstein equations,

$$G_{\mu\nu} = 8\pi G T_{\mu\nu} \tag{2.10}$$

2.2 The plane wave solution

We continue working in the weak field approximation of the Einstein action, which leads us to the Fierz-Pauli action for $h_{\mu\nu}$ [19],

$$S = \int d^D x \left[\begin{aligned} -\frac{1}{2}\partial_\lambda h_{\mu\nu}\partial^\lambda h^{\mu\nu} + \partial_\mu h_{\nu\lambda}\partial^\nu h^{\mu\lambda} - \partial_\mu h^{\mu\nu}\partial_\nu h \\ + \frac{1}{2}\partial_\lambda h \partial^\lambda h - \frac{1}{2}m^2\left(h_{\mu\nu}h^{\mu\nu} - h^2\right) \end{aligned} \right] \tag{2.11}$$

This can be reduced for $m = 0$ to,

$$\begin{aligned} S_{m=0} &= \int d^D x \left[-\frac{1}{2}\partial_\lambda h_{\mu\nu}\partial^\lambda h^{\mu\nu} + \partial_\mu h_{\nu\lambda}\partial^\nu h^{\mu\lambda} - \partial_\mu h^{\mu\nu}\partial_\nu h + \frac{1}{2}\partial_\lambda h \partial^\lambda h \right] \\ &= \int d^D x \left[\frac{1}{2} h_{\mu\nu} \mathcal{E}^{\mu\nu,\alpha\beta} h_{\alpha\beta} \right] \end{aligned} \tag{2.12}$$

which contains the familiar Lagrangian [7]. By fixing the gauge freedom using the de Donder gauge, given by,

$$\partial^\mu h_{\mu\nu} - \frac{1}{2}\partial_\nu h = 0 \tag{2.13}$$

the equations of motion of the linearized wave equation in this metric and these coordinates is now given by,

$$\Box \left[h_{\mu\nu} - \frac{1}{2}\eta_{\mu\nu} h \right] = -16\pi T_{\mu\nu} \text{ and } \partial^\mu \left[h_{\mu\nu} - \frac{1}{2}\eta_{\mu\nu} h \right] = 0 \tag{2.14}$$

and its solution by,

$$h_{\mu\nu} - \frac{1}{2}\eta_{\mu\nu} h = A_{\mu\nu} e^{i k_\rho x^\rho} \tag{2.15}$$

for $k^\mu = (\omega, \vec{k})$ with the condition that these waves propagate at the speed of light, or $\eta^{\mu\nu} k_\mu k_\nu = 0$. We will use the wave equation of Eq. (2.15) to characterize all our waveforms, and in particular will introduce phenomenological parameters to the phase term to see how these affect the dispersion of the wave. Though we have derived a plane wave solution travelling at the speed of light by assuming Lorentz-invariant transformations,

the introduction of modified parameters will necessarily violate such an assumption. As a result, the introduction of modified phase parameters is equivalent to a violation of Lorentz symmetry, and the propagation of gravitational waves at some $v_g \neq c$. Although the gauge choice is not uniquely defined, it is useful for relating the initial 10 degrees of freedom of the system to the 2 standard polarization modes for gravitational waves. In particular, of the initial degrees of freedom, the coordinate choice fixes 4 and the gauge choice another 4, leaving 2 independent degrees of freedom.

2.3 Standard polarization modes

We define the transverse-traceless (TT) gauge as one which transforms the polarisation tensor $A_{\mu\nu}$ such that:

$$\begin{aligned} A^{\mu}_{\mu} &= 0 \\ A_{\mu\nu}k^{\nu} &= 0 \end{aligned} \tag{2.16}$$

These conditions imply $A_{\mu 0} = 0$. Assuming, without any loss of generality, that the gravitational wave propagation is in the z-direction, $k^{\mu} = \omega(1, 0, 0, 1)$, we can conclude $A_{\mu z} = 0$ for all μ [20]. Together, this satisfies the transverse condition. To eliminate the A_{xx}, A_{xy} and A_{yy} components we note that the condition of (2.16) is such that $A_{yy} = -A_{xx}$.

We are left with an $A_{\mu\nu}$ that is both transverse and traceless, as desired:

$$A^{(TT)}_{\mu\nu} = \begin{pmatrix} 0 & 0 & 0 & 0 \\ 0 & A_{xx} & A_{xy} & 0 \\ 0 & A_{xy} & -A_{xx} & 0 \\ 0 & 0 & 0 & 0 \end{pmatrix} \tag{2.17}$$

We can label these components so they correspond to the physical polarization states observed for a gravitational wave, namely plus and cross:

$$\begin{aligned} A_{+} (&= A_{xx} = -A_{yy}) \\ A_{\times} (&= A_{xy} = A_{yx}) \end{aligned} \tag{2.18}$$

Finally, combine Eq. (2.15) and Eq. (2.18) and substitute the result into Eq. (2.17) to

describe a gravitational wave using its standard polarization modes,

$$\begin{aligned} h^{TT}_{\mu\nu} - \frac{1}{2}\eta_{\mu\nu}h &= h_+ + h_\times \\ &= A_{xx}e^{ik_\rho x^\rho} + A_{xy}e^{ik_\rho x^\rho} \\ &= \begin{pmatrix} 0 & 0 & 0 & 0 \\ 0 & h_+ & h_\times & 0 \\ 0 & h_\times & -h_+ & 0 \\ 0 & 0 & 0 & 0 \end{pmatrix} \end{aligned} \tag{2.19}$$

2.4 The modified dispersion relation

Now that we have derived a way of expressing a gravitational wave using its standard plus and cross polarizations, we can ask ourselves how the wave propagates as a combination of those modes. It is useful here to define a dispersion relation, and to note that under GR gravitational waves do not experience dispersion.

We begin by considering a typical dispersion relation and introducing parameters to modify it in a general, phenomenological way. A dispersion relation is simply the relation between the momentum, $p = \frac{\partial S(x,t)}{\partial x}$, and energy, $E = \frac{-\partial S(x,t)}{\partial t}$, of an extremized system where the action is labelled $S(x,t)$. We use a form motivated by the parameters we hope to use in the model, $\mathbb{A}$ and α:

$$E^2 = p^2c^2 + m_g^2c^4 + \mathbb{A}p^\alpha c^\alpha \tag{2.20}$$

where m_g is the graviton mass [21][22] and $c \neq 1$. This can be rewritten to solve for the velocity v_g at which gravitational waves propagate in the framework of a massive graviton carrying the wave. We set $\mathbb{A} = 0$ and $\alpha = 2$ as this does not yet require phenomenological modification, and write.

$$E^2 - m_g^2c^4 = p^2c^2 \tag{2.21}$$

Since velocity is defined by $v = \frac{c^2p}{E}$, we can substitute the expression $p_g = \frac{v_gE_g}{c^2}$ for the momentum of the graviton into Eq. (2.21) and divide through by E_g, its energy, to find,

$$1 - \left[\frac{m_gc^2}{E^2}\right]^2 = \left[\frac{v_g}{c}\right]^2 \tag{2.22}$$

which gives the velocity relative to the speed of light, and which approaches unity as the

graviton mass goes to the fiducial point, $m_g = 0$. For a massive graviton, the wave will undergo dispersion and propagate at this velocity v_g [23]. As explained by Mishekari et al. [22], the dispersive effects in wave propagation are equivalent to incorporating the parameters α and (to first order) $\mathbb{A}$ into a modified dispersion relation,

$$\begin{aligned}\left[\frac{v_g}{c}\right]^2 &= 1 - \left[\frac{m_g c^2}{E^2}\right]^2 - \frac{\mathbb{A}}{E^2}\left[E\frac{v}{c}\right]^\alpha \\ &= 1 - \frac{m_g^2 c^4}{E^2} - \mathbb{A}E^{\alpha-2}\left[\frac{v}{c}\right]^\alpha \\ &= 1 - \frac{m_g^2 c^4}{E^2} - \mathbb{A}E^{\alpha-2}\left[\sqrt{1 - \frac{(m_g^2 c^4}{E^2}) + \mathcal{O}(\mathbb{A}^2)}\right]^\alpha \\ &= 1 - \frac{m_g^2 c^4}{E^2} - \mathbb{A}E^{\alpha-2}\left[1 - \frac{(m_g^2 c^4}{E^2})\right]^{\alpha/2}\end{aligned} \tag{2.23}$$

This relation simplifies to,

$$\left[\frac{v_g}{c}\right]^2 = 1 - \left[\frac{m_g c^2}{E^2}\right]^2 - \mathbb{A}E^{\alpha-2} \tag{2.24}$$

in the limit where $E \gg m_g$, it is straightforward to relate the phenomenological parameter relationship to whether the graviton travels at faster or slower than the speed of light, i.e. the fiducial speed $v = c$ for general relativity. In particular, for positive $\mathbb{A}$, or more precisely $(m_g/E)^2 > \sqrt{|\mathbb{A}|E^{\alpha-2}}$, we have $v_g < c$.

Recall the general form for phase is given by $\Psi = [i2\pi f - vt]$ for a traveling sinusoidal wave. Then, it is possible to dephase this wave by treating it as a stream of particles (in our case, gravitons moving along geodesics) which travel at Eq. (2.24). Doing so is equivalent to modifying the velocity term at each frequency by this linear relation. When considering how to define the cosmological distances over which these particles travel, it becomes necessary to introduce an intermediate term to account for apparent differences in distance travelled as measured in phase changes at a given frequency; there will be more on this in the derivation of modified luminosity distance in Section 3.2.

We define the wavelength $\lambda_{\mathbb{A}} = h\mathbb{A}^{1/(\alpha-2)}$ to describe where effects peak in ω because, in general, there should be visible phase coherence for $\omega \sim \lambda_{\mathbb{A}}$. We can use $\lambda_{\mathbb{A}}$ to relate the graviton mass to the frequency of the gravitational wave signals. Specifically, we consider,

$$m_g = E_e\left[\frac{1}{\lambda_g f_e}\right] \tag{2.25}$$

and substitute in the emitted gravitational wave frequency, $f_e = E_e/h$, which reduces Eq. (2.9) to $m_g = h/\lambda_g \rightarrow \lambda_g = h/m_g$, which we can identify with the Compton wavelength for this particle.

This outlines how introducing phenomenological parameters will modify the traditional dispersion relation for a gravitational wave. These changes should be detectable [24] for a waveform propagating over cosmological distances. To fully characterize the dispersion relation, it may be necessary to account for changes in group velocity due to individual eigenstate distortions [25], but that remains outside the scope of this project.

2.5 Frequency-dependent approach

2.5.1 Telescopes and detectors

The nature of gravitational waves necessitates highly calibrated and sensitive instruments to place reasonable detection limits on signals. LIGO accomplishes this by combining laboratories on different continents into an effectively Earth-sized aperture [3]. This observatory detects signals in the $10^1 - 10^4$ Hz.

The next range in frequencies to be probed will be the microhertz bands, which will be covered by the Laser Inferometer Space Antenna (LISA), due for launch in the 2030s [26]. LISA, will look for signals from black holes around the time of the first stars, and directly map the curvature of spacetime around their event horizons. In doing so, it will test the strong-lensing interactions [26] around early, quiescent black holes [27], and search for anisotropies from the early universe [28]. Also slated for launch in the 30s are the Einstein Telescope and the Cosmic Explorer, which will look for compact objects which do not immediately inspiral [29]. These may be able to provide extra sources in the bands we study, and will be useful for corroborating the behavior of signals measured by LIGO.

For example, the chirp masses of Intermediate Mass Black Holes (IMBHs), around 10^2-10^5 $M_\odot$, are among the most difficult to detect because the frequency emitted by their mergers sits on the edge of the sensitivity band for LIGO (except for very small redshift, on the order of $z < 0.1$) [30]. Their emitted frequency is, however, precisely within the optimal range for detection by LISA. This means that LISA will provide a chance to see objects that LIGO does not, though again our focus will be on tracking gravitational waves as they evolve between the sensitivity bands of multiple detectors.

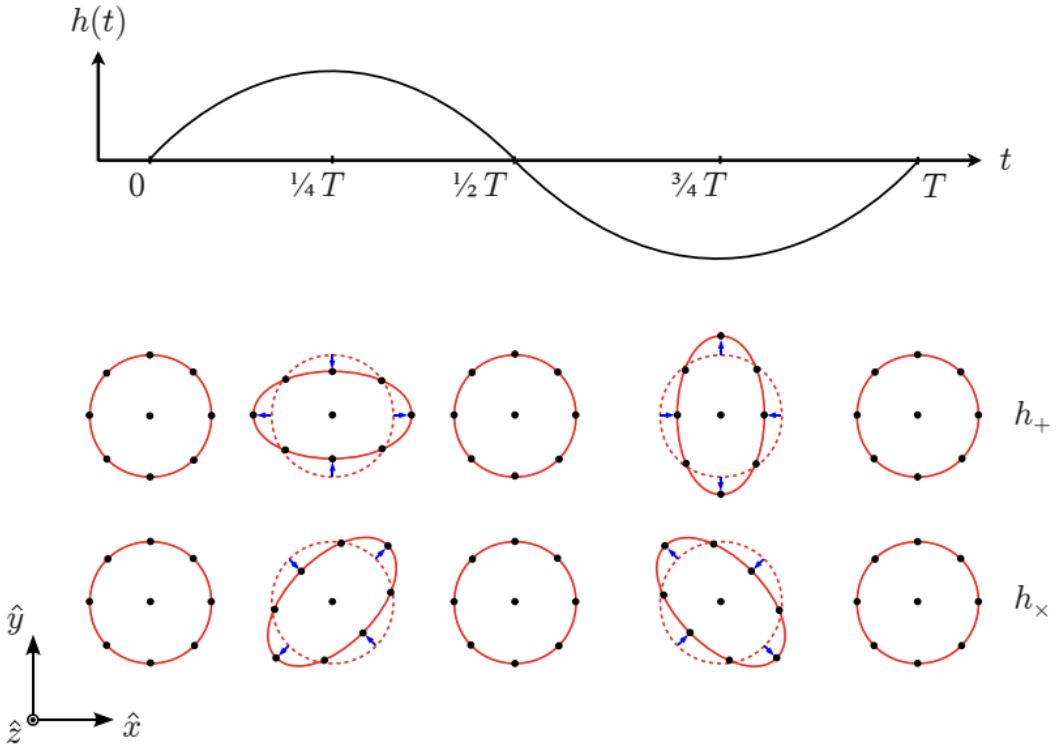

Figure 2.1: Diagram showing interaction between an incoming gravitational wave polarized along the z-direction and a laser inferometer situated in the xy-plane. The $+$ and $\times$ polarizations are given based on how these would distort a circle of freely-falling particles, and these distortions are matched to the corresponding point in the period T of propagation. A GW detector would observe this change due to the interference of the gravitational wave with the light wave from its laser beams. Taken from [20].

Fortunately, whether the gravitational wave observatory is on Earth or in space, the basic mechanism for detecting signals is the same. To start, the design of LIGO involves two arms of 4km each which stretch out at a 90°angle and which have laser beams passing back and forth. Suppose these arms are aligned on the xy-plane, and a gravitational wave passes transverse to this plane. The gravitational wave distorts spacetime as it passes through the detector, which shows up as a change in the time it takes the lasers to travel. Otherwise, the light beams superimpose and cancel.

Based on the polarization mode of the wave, described in Section 2.3, the detector will register differences in the time it takes both waves to travel, due to the stretching or compression of the phase [31]. A schematic of this can be seen in Fig (2.1), which assumes the same geometry we do and where the period T is given by $T = 2\pi/\omega = 1/f$.

In the case of LISA, there will be a triangle of satellites in a carefully maintained formation orbiting Earth. Notably, this will introduce a solid angle parameter to integrate the signal sensitivity over [32]. The individual satellites will each contain two test masses whose position will be resolved using interferometry, and this will form the basis of measuring incoming gravitational waves [31].

Chapter 3

Assembling and testing waveforms

3.1 Approximating numerical general relativity

General relativity can be approximated computationally using a full numerical implementation. Full numerical general relativity has the highest degree of precision [33][34], but is not always viable given the cost of running a full numerical program for a large set of waveforms. We must therefore forgo some acceptable level of accuracy in order to build a usable model. One of the most commonly used approximations is the post Newtonian (PN) expansion detailed below, and in particular the `TaylorF2` parametrization of the approximant waveform [35][36].

To give an analogy: we can think of this model as a sort of bridge. The purpose is to ferry us from the traditional theoretical framework of the previous chapter to a set of constrained parameters representing a new framework. This requires making a choice as to what is brought with us and what is left behind, for example, some accuracy in the form of high-order terms and computer precision is sacrificed. Instead, we make reasonable approximations where appropriate and use these to represent the underlying dynamics of the system.

3.1.1 The post Newtonian (PN) expansion

The optimal trade-off for our purposes is to use the 3.5PN (post Newtonian) approximation as implemented by Buonanno et al. [35], which may seem counter-intuitive for

research involving gravitational waves. However, this approximation has been shown to be consistent with observation and full numerical GR [37]. There has been speculation that the underlying reason is a redshift effect which makes strong gravity appear weaker to observers far away [37]. We should recall also that we are working in the weak field approximation of GR and so, for our purposes, a PN approximation is justified.

It is possible to translate the theoretical derivations in the second chapter to a numerical description that uses this 3.5PN approximation. The general phenomenological form of the waveform Eqn. (2.15) is given by,

$$\tilde{h}(f;\vec{\lambda},\vec{\theta}) = \tilde{A}(f;\vec{\lambda})e^{i\tilde{\Psi}(f;\vec{\theta})} \tag{3.1}$$

where $\vec{\theta}$ is a vector representing the phase parameters and $\vec{\lambda}$ the same for amplitude [38]. This holds for a frequency interval below some cutoff f_{max} at which the approximation fails. There is also an f_{min} for which there is insufficient sensitivity to separate noise, and it is described in more detail later on. The values of f_{max} and f_{min} depend on the detector measuring the gravitational wave and can be found in Table 3.1. From these relationships we can see that the frequency bands studied here are determined by the approximation used, noise and signal model, and detector sensitivity.

In our model, modification parameters are restricted to the phase (which is called the restricted PN approximation [22]) and so Eqn. (3.1) simplifies to,

$$\tilde{h}(f;\vec{\theta}) = \tilde{A}(f)e^{i\tilde{\Psi}(f;\vec{\theta})} \tag{3.2}$$

The two are equivalent in the sense that they generally describe the same physical phenomena, though the theoretical equation is more representative of nature and the numerical equation more relevant to studying the system. Going forward, we will use this definition of the waveform.

A note about the choice of parametrization. We have already said the `TaylorF2` approximant is one of the most popular, and that, for our model, it makes sense to work in the frequency domain. It is also worth mentioning how the approximant is generated. As the name suggests, it relies on a Taylor series expansion of the velocity $v = (\pi M f)^{1/3}$ in the phase term of the waveform. This is the case for all of the Taylor PN approximants (compare to `IMRPhenomA`, which instead uses a phenomenological formulation [39]). The `F2` and `T2` refer to frequency and time respectively, and to the second form of the adiabatic phasing relations outlined in [35].

	Adv. LIGO	LISA	ET
f_{min}	10 Hz	10^{-5} Hz	1 Hz
f_{max}	10^4 Hz	1 Hz	10^5 Hz
ϵ	1	$\sqrt{3}/2$	1

Table 3.1: Cutoff (measured) frequencies for different classes of detector. These are important for determining the range within which our model is effective. Also shown are the values of ϵ, a constant accounting for the detector geometry and relevant for the waveform amplitude terms.

3.1.2 The Stationary Phase Approximation (SPA)

A stationary phase approximation (SPA) is used to produce an analytic solution to the Fourier transform of a waveform. The approximation effectively assumes that all time dependence is in the phase of the wave, and thus is valid when the phase changes much faster than the amplitude does. Hence, it avoids computing the Fourier transform of a nonlinear term. It is a robust approximation to use; in fact, it can be shown that second-order corrections to the SPA are sufficiently small so as to be discarded [40], and due to the time windowing rather than a failure of the approximation itself.

Though the model takes in and modifies `PyCBC` waveforms, it is necessary to ensure the modifications themselves behave as expected. It is easy to see the modifications produce changes by comparing the input waveforms to the output, but how do we ensure those changes are only the ones we want? We start by generating unmodified signals in house, and convincing ourselves these recreate the `PyCBC` waveforms. As expected, the waveforms produced in house correspond well to those generated by `PyCBC`, but the exercise is a useful one as there are constants of integration due to the Fourier transform and scaling corrections that arise.

3.2 Modified luminosity distance

We now turn to a definition of a modified luminosity distance, useful for parametrizing the modified signal as a function of redshift and understanding precisely how it changes while traveling from the system to the detectors.

To do so, let us introduce the cosmological principle, which states the universe is the same for all observers on scales of roughly $\gtrsim 100$ Mpc. This is equivalent to saying the universe is

homogeneous (obeys translational symmetry) and isotropic (obeys rotational symmetry), on these scales. Together, these assumptions give rise to the Friedman-Robertson-Walker (FRW) metric:

$$ds^2 = -dt^2 + a^2(t)\left(\frac{dr^2}{1-Kr^2} + r^2 d\theta^2 + r^2 sin^2\theta d\phi^2\right) \tag{3.3}$$

where (r, θ, ϕ) are spherical coordinates, r is the co-moving radial coordinate, K is the curvature constant, and $a(t)$ is the scale factor [5]. Note this implies the only expansion admitted is expansion or contraction which is the same in all directions. From here we can obtain a new expression for the modified dispersion relation first encountered in Eq. (2.20) [41],

$$g_{\mu\nu}p^\mu p_\nu = -E^2 + \delta_{ij}a^2 p^\mu p_\nu = -m_g^2 + \mathbb{A}|p|^\alpha \tag{3.4}$$

where the momentum,

$$p^\mu = \big(E, k/a^2, 0, 0\big) \tag{3.5}$$

has been redefined in terms of the metric, $|p| = \sqrt{(g_{ij}p^i p_j)} = k/a^2$ for the comoving wave number k and scale factor a. This reduces to the standard dispersion relation for massless m_g. Then, we suppose a graviton is emitted at $r = r_e$ and, since spherical coordinate symmetries confine its movement to the radial component of the trajectory, we disregard the others and receive it at $r = 0$.

Next, since the scale factor a is related directly to the particle momentum by,

$$p_r^2 = a^2(t)(E^2 - m_g^2 - \mathbb{A}|p|^\alpha) \tag{3.6}$$

we can rewrite the usual luminosity distance to a more useful metric for our parameter α. In fact, the luminosity distance defined for the FRW metric in general relativity can be adjusted for gravitational waves propagation in a theory of modified gravity. This is done to avoid the distances for gravitational waves being effected by a dark energy equation of state [42]).

Recall that luminosity distance arises from the relationship between flux, distance, and the known luminosity of an object:

$$F = \frac{L}{4\pi d^2} \tag{3.7}$$

where for a comoving system, the denominator is best expressed using a term with scale

factor dependence, $\chi(a)$,

$$\chi(a) = \int_{t(a)}^{t_0} \frac{dt'}{a(t')} \tag{3.8}$$

To account for the fewer photons passing through a spherical shell in such a setup, a factor of $a^2 = 1/(1+z^2)$ is introduced to the numerator. Together, these lead to the adjusted expression,

$$F = \frac{La^2}{4\chi^2(a)} \tag{3.9}$$

We can see that the original form of Eq. (3.7) is recovered for a luminosity distance given by $D_L = \chi/a$ We can equivalently express the χ term as a function of redshift [41],

$$\chi(z) = \int_0^z \frac{dz'}{H(z')} \tag{3.10}$$

by making use of the Hubble parameter $H(z)$. Then, using $H(z) = H_0 E(z)$ to relate the Hubble parameter to the Hubble function [5],

$$E(z) = \sqrt{\Omega_r(1+z)^4 + \Omega_m(1+z)^3 + \Omega_k(1+z)^2 + \Omega_\Lambda} \tag{3.11}$$

we have:

$$\begin{aligned} D_L &= \frac{\chi}{a} \\ &= (1+z)\int_0^z \frac{dz'}{H\left(z'\right)} \\ &= \frac{(1+z)}{H_0}\int_0^z \frac{dz'}{E\left(z'\right)} \\ &= \frac{(1+z)}{H_0}\int_0^z \frac{dz'}{\sqrt{\Omega_m(1+z)^3 + \Omega_\Lambda}} \end{aligned} \tag{3.12}$$

The Ω_k term has been removed because our universe has approximately flat curvature, i.e. $K = 0$ in Eq. (3.3) above; $\Omega_r = 0$ because the universe evolved away from its radiation-dominated phase before the gravitational wave sources we consider formed [5]. Thus we have an expression for luminosity distance that agrees with our concordance universe.

This can now be modified to produce a luminosity distance D_α,

$$D_\alpha = \frac{(1+Z)^{1-\alpha}}{H_0}\int_0^Z \frac{(1+z')^{\alpha-2}\,dz'}{\sqrt{\Omega_M\left(1+z'\right)^3 + \Omega_\Lambda}} \tag{3.13}$$

Such a distance metric is useful for calculating distances with the Lorentz-violating terms that modify the gravitational wave signals in our phenomenological model. These are

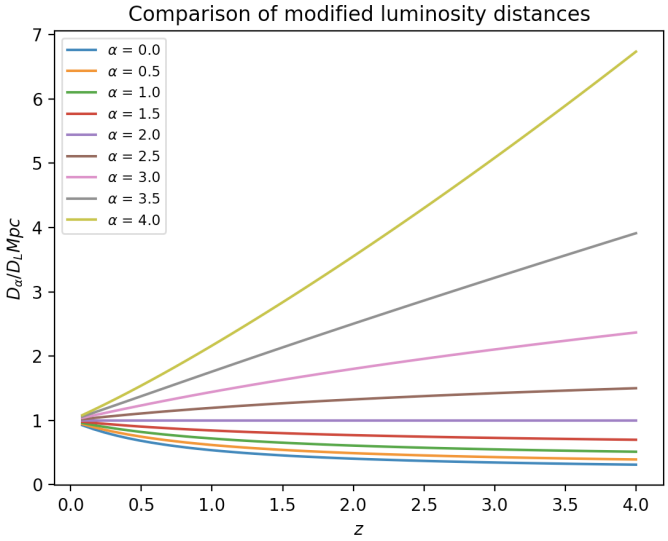

Figure 3.1: The effect of the α parameter on luminosity distance plotted relative to standard luminosity distance as a function of redshift. Notably, the ratio is $D_\alpha/D_L = 1$ when $\alpha = 2$, as this corresponds to a cancellation of the modified portion of the dispersion relation.

numerous and outlined in Table 1.1. As an example, the ratio D_α/D_L is plotted against redshift in Fig. (3.1).

3.3 Relationship between standard $\prec$ modified amplitude and phase terms

It is useful here to describe exactly what the standard and modified waveforms look like and how the modified waveform can be reduced to its standard counterpart. The standard waveform,

$$h(f) = A_S(f)e^{i\Psi_S(f)} \tag{3.14}$$

can be defined using its amplitude and phase [21], where

$$\begin{aligned} A_{\rm S} &= \sqrt{\frac{\pi}{30}}\frac{\mathcal{M}^2}{D_L} \\ \Psi_{\rm S}(f) &= 2\pi f t_c - \Phi_c - \frac{\pi}{4} + \frac{3}{128}u^{-5/3} \times \sum_{n=0}^{\infty}\left[c_n + \ell_n \ln(u)\right] u^{n/3} \end{aligned} \tag{3.15}$$

These are modified by introducing a mass term $u = \pi\mathcal{M}f = v^3$ where v is the orbital velocity and a coefficient ϵ (see Table 3.1) to the amplitude and a $\delta\Psi(f)$ term to the phase. The power of the mass term is determined by the 3.5PN order approximation where the c_n coefficients stop at $n = 7$ [35]. This is because, in general, PN approximations account for relativistic effects through an expansion parameter $\xi = v^2/c^2$ and the phase expansion degree for 3.5PN stops at v^7 [38]. These terms are important but the non-GR components are those in the $\delta\Psi(f)$ phase contribution, and so we will focus on those.

Now, the modified waveform is defined analogously to Eq. (3.14) as,

$$\tilde{h}(f) = A_M(f)e^{i\Psi_M(f)} \tag{3.16}$$

where the amplitude and phase terms are now given by the following [22],

$$\begin{aligned} A_{\mathrm{M}} &= \epsilon u^{-7/6} A_{\mathrm{S}} = \epsilon u^{-7/6}\sqrt{\frac{\pi}{30}}\frac{\mathcal{M}^2}{D_L} \\ \Psi_{\mathrm{M}}(f) &= \Psi_{\mathrm{S}}(f) + \delta\Psi(f) \\ &= \begin{cases} \Psi_{\mathrm{S}}(f) - (\beta u^{-1} - \zeta_{\alpha=1}\ln(u)) & \text{for } \alpha = 1 \\ \Psi_{\mathrm{S}}(f) - (\beta u^{-1} + \zeta u^{\alpha-1}) & \text{otherwise} \end{cases} \end{aligned} \tag{3.17}$$

In particular, the term depends on factors caused by dephasing – precisely those which we are interested in constraining. These are listed in Table 3.2 and correspond directly to the value of the dispersion term α, which varies between $(0, 4)$ in discrete steps of .5 and reduces to the standard dispersion relation when $\alpha = 2$. In this case, the α is a renormalization factor of c and the $\mathbb{A}$ correction to $\lambda_{\mathbb{A}}$ is no longer frequency-dependent [43]. There is therefore a mapping between the modified dispersion relation and the phenomenological parameters, as illustrated in Fig. (3.2). This inspires our approach to constraining the modified dispersion relation and our focus on frequency-dependent effects.

3.3.1 Confirming standard waveform behavior prior to introducing phenomenological parameters

One important step was to construct the standard waveforms in-house before switching these out for their `PyCBC` counterparts. This was important to ensure any modifications performed on the waveform behave as they should. Not only did this check the modified

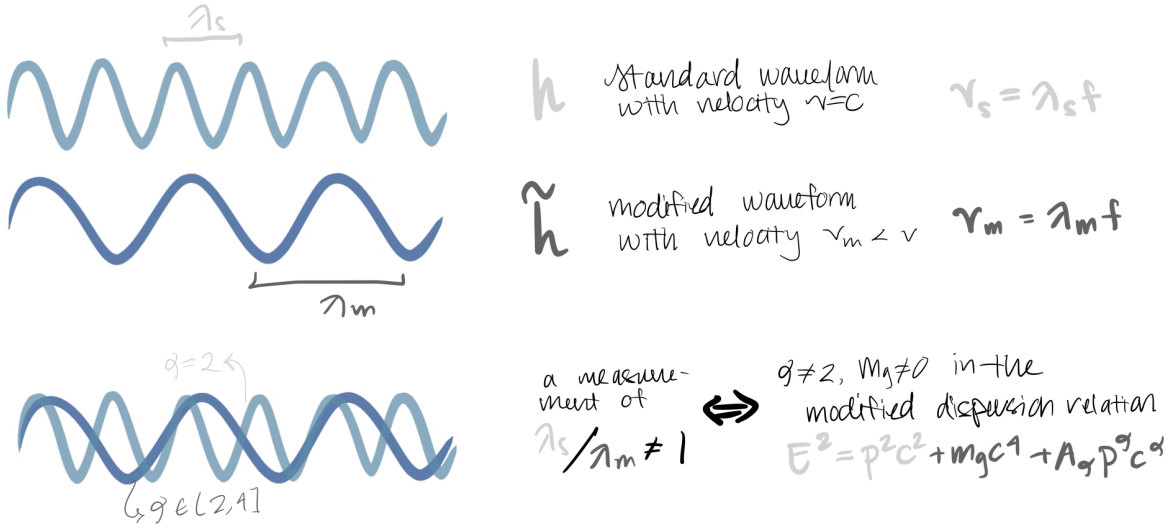

Figure 3.2: Illustration of the relationship between the standard and modified wavelengths λ_s and λ_m, their associated velocities v_s and v_m, and the resulting waveforms h and $\tilde{h}$. We note the modified dispersion relation simplifies to the standard, relativistic one where there is no dispersion present. This is consistent with general relativity predicting no dispersion for gravitational waves [44]. Note the standard forms are given in light blue and grey, and the modified components in dark blue and grey.

Term	Expression	Description	in GR
m_g	$E_e(\lambda_g f_e)^{-1}$	Massive graviton	0
α	1, 1.5, 2, 2.5, 3, 3.5, 4	Exponent for momentum component of dispersion relation	2
$\mathbb{A}$	$(\lambda_{\mathbb{A}}/h)^{\alpha-2}$	Coefficient for momentum component of dispersion relation	0
λ_g	h/m_g	Wavelength associated to m_g	∞
$\lambda_{\mathbb{A}}$	$h\mathbb{A}^{1/(\alpha-2)}$	Wavelength associated to $\mathbb{A}$	0
u	$\pi\mathcal{M}f$	Dimensionless mass factor	-
β	$\frac{\pi^2 D_0 \mathcal{M}}{\lambda_g^2(1+Z)}$	Non-linearity measure	1
ζ	$\alpha \neq 1 : \frac{\pi^{2-\alpha}}{(1-\alpha)} \frac{D_\alpha}{\lambda_{\mathbb{A}}^{2-\alpha}} \frac{\mathcal{M}^{1-\alpha}}{(1+Z)^{1-\alpha}}$ $\alpha = 1 : \frac{\pi D_1}{\lambda_{\mathbb{A}}}$	Effects due to preferred location	0

Table 3.2: Phenomenological and Lorentz-violating terms used to modified the dispersion relation.

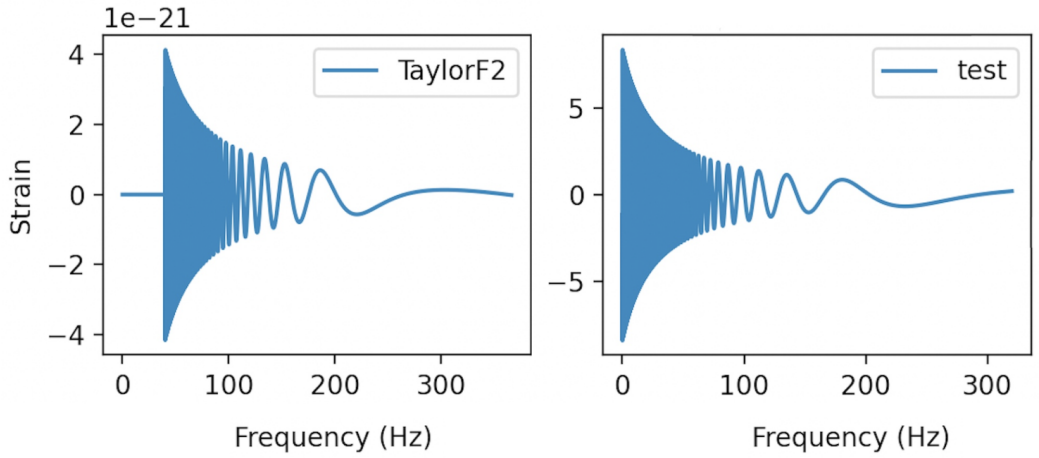

Figure 3.3: Strain (amplitude) of two standard waveforms plotted over the a typical frequency range for LIGO to demonstrate in-house waveforms are reasonably similar to those from `PyCBC`. TOP: The `TaylorF2` approximant generated from `PyCBC`. BOTTOM: The 'test' waveform built in house with no modifications. Though there is a normalization factor offset which contributes to the tail missing from the bottom waveform, the two have the same amplitude behavior.

waveforms differed only through phenomenological changes, it confirmed the modified waveform of Eq. (3.16) reduces to its standard form in a straightforward manner. The main point of disagreement was due to a normalization choice of $\frac{1}{\sqrt{n}}$ in the inverse Fourier transform of the signal to the time domain and an order of magnitude discrepancy due to ϵ-scaling. Once these was adjusted for, the in-house waveforms matched those of `PyCBC` sufficiently well, as seen in Fig. (3.3). This exercise convinces us any changes in behavior the modifications reveal are due to a physical difference and not a perceived one.

3.3.2 The modified waveform: troubleshooting problems

In order to establish the waveform evolved correctly overall, we used the inner product relationship between the amplitude and phase terms to check each separately in frequency space. The `PyCBC` waveforms use an underlying `SciPy` function to perform the inverse Fourier transform. A point of trouble here arose from saving the modified signal to two separate arrays, where the real and complex portions were assigned separately. This lead to the complex portion being returned as a real array, equivalent to losing the phase information [45]. This was noticed by using an inner product calculation to separate phase

and amplitude, and plotting the evolution of both, shown in Fig. (3.4). From these plots, it was evident that the phase was not undergoing any change in time, and obviously the phase information was not being stored properly. This was easily fixed by adding the imaginary component back in to the array, and the result was a correctly-modified waveform.

The inner product factorization was found using,

$$\frac{\Phi(f) = A(f)e^{i\psi(f)}}{\sqrt{|\Phi^2(f)|}} \tag{3.18}$$

where the phase $\Psi = (\Psi_{\rm GR}, \Psi_{\texttt{PyCBC}})$ and the amplitude,

$$\sqrt{|\Phi^2(f)|} = \sqrt{\Phi(f)\Phi^*(f)} = A(f) \tag{3.19}$$

Combining Eqns. (3.18) and (3.19) we write an expression for the real component of the `PyCBC` library waveform phase,

$$\Psi_{\texttt{PyCBC}}(f) = \cos^{-1}\left[\frac{\Phi(f)}{\sqrt{|\Phi^2(f)|}}\right] \tag{3.20}$$

This is plotted against a frequency band typical of a LIGO-observed gravitational wave in Fig. (3.4).

The inner product check was useful also because it revealed an issue with the amplitude evolution that may not have otherwise been detected. In particular, the amplitude term of Eq. (3.17) may at first appear to be constant in frequency. This is not the case, and the form of the gravitational wave envelope shows a change in amplitude over frequency and indeed this frequency dependence is *implicitly held in the luminosity distance term.* The code was fixed by introducing the relevant frequency dependence by passing through an array of redshifts, where $z = \Delta f/f$ to the standard amplitude term.

We next check the waveforms can be translated between the time and frequency domains using Fourier transforms. This involves saving the waveform as a `PyCBC` object of type `TimeSeries` where the sampling is in the time domain (t_0, t_f) and type `FrequencySeries` where it is in the frequency domain (f_0, f_f) for $f_0 \geq f_{min}$ for the relevant detector-based values as given in Table 3.1. Note the f_{max} cuttoff can be ignored since there is no need to use the PN approximation to confirm waveform can be translated between time and frequency domains. Instead, we use the non-spin phenomenological approximation,

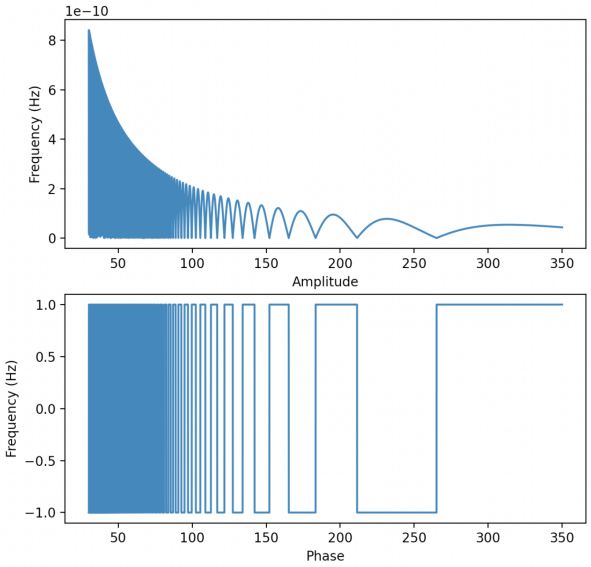

Figure 3.4: Frequency peaks and evolution of `IMRPhenomA` waveform, separated into its amplitude and phase components.

`IMRPhenomA`, and the main assumption made is that changes in amplitude outpace those in phase as explained in Section 3.1.2.

The main difficulty in transforming between time and frequency domains was due to not being able to debug the arrays once these were made into `PyCBC` objects. Since `PyCBC` embeds the `SciPy` into its Fourier and inverse Fourier transform functions, we stored waveforms as arrays, performed the necessary (inverse) Fourier transforms by making a direct call to `scipy.fft.(i)fft`, verifying behavior, and then storing as types. The last part was necessary to check that not only did the waveforms transform correctly between domains, but they could be absorbed into the `PyCBC` framework for straightforward integration.

3.3.3 Characterizing the modified signal

The resulting modification can be visualized as a birefringence of the circular plus and cross polarizations traditionally associated with gravitational waves [46]. That is, the modified dispersion of the waves will appear anisotropic with respect to direction [47].

Since dispersion relation for gravitational waves are well-constrained, it is likely that any information in the modified signal will appear in the form of a fractional change [48]. We

thus compare the ratio of modified to standard amplitudes and test parameters in their limits. This allows us to set a reasonable bound for expected behavior but not to conclude that the observed behavior will produce the same magnitude effects.

3.4 Fisher analysis

When gravitational wave data is received at a detector, the signal is obscured by noise. By developing a basic methodology for extracting the signal from the data, we can isolate the desired information. This involves considering the signal and noise components separately,

$$D(t) = S(t) + N(t) \tag{3.21}$$

and in particular their representation in frequency space,

$$\begin{aligned} \tilde{D}(f) &= \tilde{S}(f) + \tilde{N}(f) \\ &\rightarrow \boldsymbol{D}_f - \boldsymbol{N}_f = \boldsymbol{S}_f \end{aligned} \tag{3.22}$$

which is found by performing a Fourier transform.

Removing contributions from noise requires constructing a noise model for the detector-specific noise power spectra P_{LIGO}, P_{LISA}. Once we have a way of describing that noise, we can perform a Fisher analysis to study the behavior of the system. To do so, we construct the Fisher matrix using partial derivatives with respect to the phenomenological parameters used to modify the waveforms.

This gives us a statistical understanding of how the waveform evolves in its parameter space with respect to the changes we apply. Bounds on the effectiveness of the phenomenological model in constraining data can be calculated from the Fisher analysis, as can degeneracies between parameters.

3.4.1 The noise power spectrum

The noise power spectral density, along with location and inclination angle, is one of the defining attributes of a gravitational wave detector [49]. It determines the frequency of data the detector is sensitive to, which generally includes signals lying about an order of magnitude above the associated sensitivity curves [50] shown in Fig. (3.5).

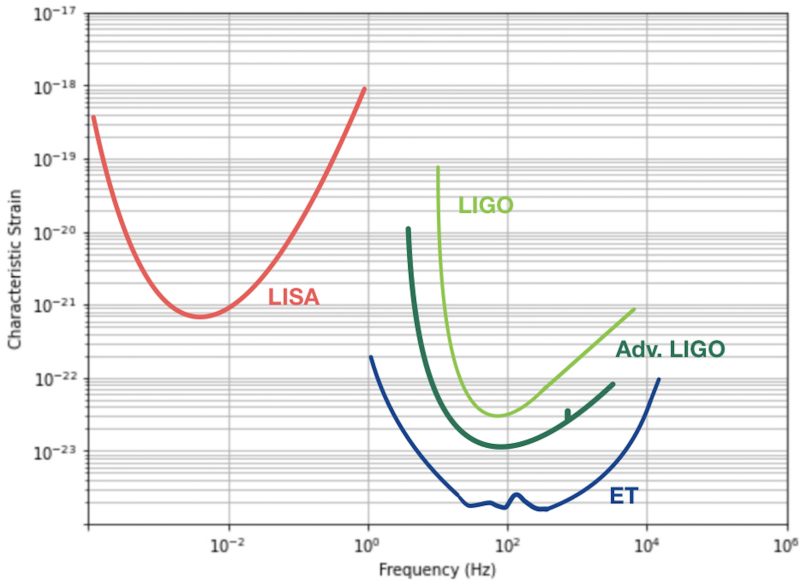

Figure 3.5: Characteristic strain h_c plotted against frequency with LISA, LIGO, Adv. LIGO, and ET sensitivity curves shown in pink, light green, dark green, and blue respectively. Adapted from data compiled from [52] [30] and [51].

By assuming the detector noise is stationary and Gaussian (with zero mean), it is possible to fully determine the noise from its power spectral density $S_n(f)$ [51],

$$(\boldsymbol{N}_f \mid \boldsymbol{N}^*_{f'}) = \frac{1}{2}\delta\left(f - f'\right) S_n(f) \tag{3.23}$$

which, due to real-valued constraints on data from GW sources and detectors implies $S_n(f) = S_n(-f)$ is an even function and can be found from integrating with respect to positive frequencies only [51]. We can see from Fig. (3.5) that $S_n(f)$ is valuable also in that it allows us to easily see which signals would be within the observatory scope of a given detector. The characteristic sensitivity strain for a detector is given by $\sqrt{\mathbb{K} f S_{\mathrm{n}}}$ where $\mathbb{K}$ is a constant, e.g. $\mathbb{K} = 4$ for LISA [50][51]. This is important because different classes of objects and different stages of a merger produce signals of different frequency, and so to have a holistic picture of the information GWs can tell us, it is necessary to observe in as wide a total frequency band as possible. Crucially for studying dispersion, the ability to track a single GW signal as it progresses through multiple frequency bands would immediately constrain propagation effects.

Sensitivity curve for Advanced LIGO

We return to considering our phenomenological approach, and plot sensitivity strains using the analytical fit developed by Mishra et al. in their paper on parametrized tests of PN theory [53].

We have, for $x = f/f_0$,

$$S_n(f) = S_0 \left[\begin{array}{l} 10^{16-4(f-7.9)^2} + 2.4 \times 10^{-62} x^{-50} \\ \qquad + 0.08 x^{-4.69} + 123.35 \left(\dfrac{1 - 0.23x^2 + 0.0764x^4}{1 + 0.17x^2} \right) \end{array} \right] \tag{3.24}$$

For Advanced LIGO and similar detectors, $f_0 = 215$ Hz, $f \in (10^0, 10^4)$ Hz, $S_0 = 10^{-49}$ Hz^{-1}, and this expression is valid for $f \geq f_s = 20$ Hz. The exact value of f_s is not particularly important, just that it serves as a reasonable low energy cutoff below which the approximation fails (i.e. below which the SNR is insufficient to isolate a signal). The upper frequency cutoff is set by a factor of v_{lso}, the velocity at last stable orbit, and depends on the source [35].

Sensitivity curve for LISA

In the case of a LISA-like detector, the $S_n(f)$ is given by,

$$S_n(f) = \sqrt{\frac{40}{3} f \left[\frac{S_1(f)}{(2\pi f)^4} + 3.6 \times 10^{-41} \right] \left[1 + \left(\frac{f}{2.5 \times 10^{-6}} \right)^2 \right]} \tag{3.25}$$

where

$$S_1(f) = 5.76 \times 10^{-48} \left[1 + \left(\frac{4 \times 10^{-7}}{f} \right)^2 \right] \text{s}^{-4} \text{ Hz}^{-1}$$

guarantees a $time \times frequency$ unit dependence such that the overall units are in *distance* as expected for amplitude.

Sensitivity curve for ET

The final design configuration of ET has not yet been decided, but the official sensitivity curve will respect the same general frequency range as Advanced LIGO: $f \in (10^0, 10^4)$

Hz. Using the same structure as Eq. (3.24) above, we have an analytical approximation to the sensitivity curve given by,

$$S_n(f) = S_0 \left[(2.39 \times 10^{-27})x^{-15.64} + 0.349x^{2.145} + 1.76x^{0.12} + 0.409x^{1.10}\right]^2 \tag{3.26}$$

Now, $f_0 = 100$ Hz and $S_0 = 10^{-50}$ Hz^{-1}.

3.4.2 The Fisher matrix and parameter choices

The Fisher matrix F_{ij} can be thought of intuitively as an exploration in parameter space of system behavior responding to changes $\frac{\partial^2}{\partial\theta_i\partial\theta_j}$ for parameters $\theta_i \in \vec{\theta}$. The vectors of F_{ij} represent directions in parameter space and the steepness of descent from some fiducial point at which the sums of partial derivatives is identically zero corresponds to how much changing a given parameter influences the system dynamics. In our case, the fiducial point is the standard gravitational wave of general relativity, and the parameters are those which we use to phenomenologically modify the waveforms. A visualization of this behavior is provided in Fig. (3.6).

Using the appropriate choice of noise power spectrum $S_n(f)$, we can compute the inner product of two waveforms,

$$(h \mid g) = 2\int_0^\infty \frac{df}{S_n(f)}\left[\tilde{h}^*\tilde{g} + \tilde{g}^*\tilde{h}\right] \tag{3.27}$$

and from this calculate the SNR of a given waveform,

$$h_{SNR} = \sqrt{(h \mid h)} \tag{3.28}$$

Assuming a large SNR, the error in some parameter θ_i is the i-th diagonal component of the Fisher matrix. This means the Fisher matrix is formally given by,

$$F_{ij} = \langle \frac{\partial^2\tilde{h}}{\partial\theta_i\theta_j} \rangle \tag{3.29}$$

for parameters θ_i, θ_j and a signal h [54]. It is useful here to explicitly state the relationship between F_{ij} and the associated parameter covariance matrix: they are inverses of each other [55]. Thus, the Fisher matrix tells us how well a set of parameters $\vec{\theta}$ can be constrained from the given data.

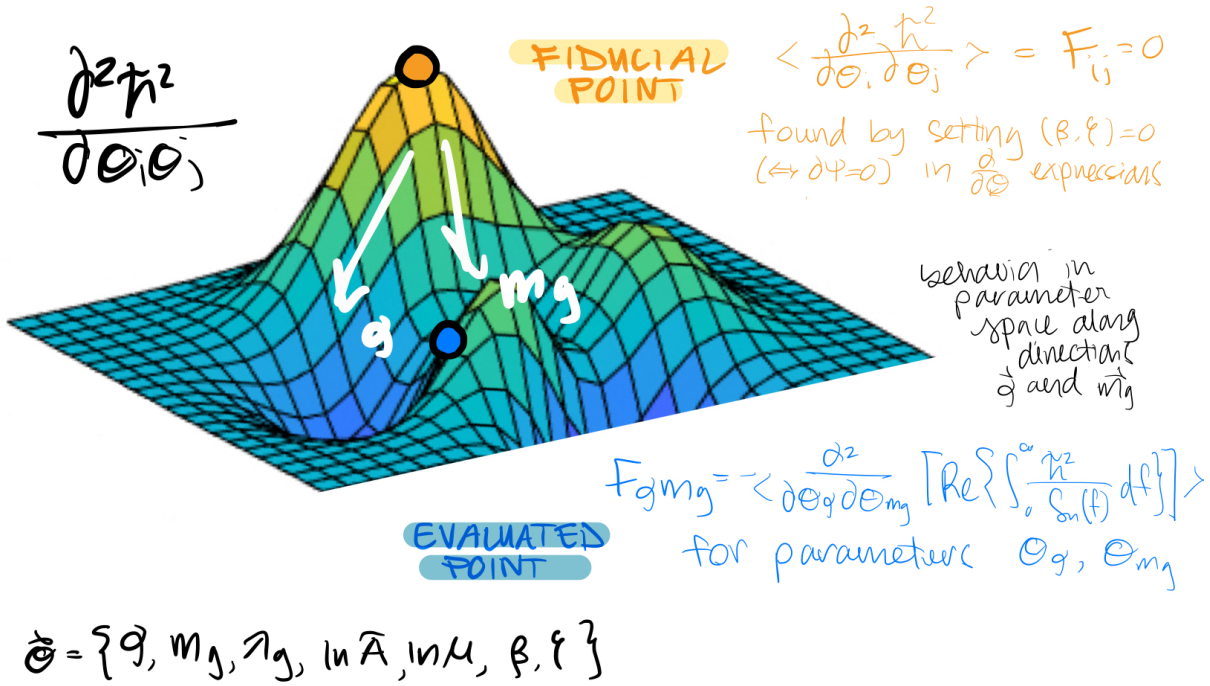

Figure 3.6: A visualization of the Fisher matrix F_{ij} showing how the contour plot evolves in parameter space. The fiducial point, labelled in orange, is the one which corresponds to general relativity and thus has all phenomenological parameters (and thus $\delta\Psi$) vanish. For clarity, only two directions $\vec{\alpha}$ and $\vec{m}_g$ are shown. The point $F_{\alpha m_g}$ at which the partial derivatives with respect to θ_α and θ_{m_g} are taken of the (real component) of the integrated signal is called the evaluated point and shown here in blue.

Correlations between different elements of $\vec{\theta}$ are given by the (nonzero) off-diagonal terms of this matrix, and the diagonal terms correspond to (the inverses of) the variances between parameters [56]. In the limit where all vectors $\partial h^2/\partial\theta_i$ are orthogonal with respect to the inner product given by the i, j components of the Fisher matrix, F_{ij}, the covariance matrix is diagonal and errors are uncorrelated [57]. Thus, lower error bounds are minimized for some θ_i if the other $\theta_0, .., \theta_{i-1}, \theta_{i+1}, ..$ are known. Indeed, for our purposes, we will assume the noise is uncorrelated which leads to a diagonal covariance matrix in detector space [55],

$$\boldsymbol{C}_{\alpha\beta} = \delta_{\alpha\beta} P_\beta \tag{3.30}$$

for P_β the power spectral density of a detector β. The frequency here is described by a Delta function with a peak corresponding to the frequency peak for the underlying timeseries. The form of the noise power spectrum motivates the frequency-dependent nature of the modifications in this model – since the noise is approximately stationary

in frequency, it is easiest to work in the frequency domain. This simplifies the task of isolating behavior to locating frequency peaks for a given waveform.

Otherwise, the minimum standard deviation increases to $\Delta\theta_i \geq (\mathbf{F}^{-1})_{ii}^{1/2}$ [57]. Given that other parameters are rarely known exactly, and must be themselves estimated from the data set, the errors do usually have some correlation. Considering the opposite limit, in which a curve can be expressed as a linear combination of other curves, the error bars are infinite for null eigenvalues [58]. This is due to a degeneracy between parameters. One of the most useful aspects of the Fisher analysis is determining which parameters are degenerate with respect to each other, because it provides a theoretical limit on how well that data can be constrained. We can use this to determine constraints for our parameters $\vec{\theta}$ and to provide an analysis of the modified waveform dispersion.

Analytical and numerical partial derivatives

Just as we had to make choices between accuracy and building a usable model when discussing approximations to numerical general relativity, we now want to calculate partial derivatives for the Fisher matrix – a process that can be both computationally costly and time-consuming. However, it is better both in terms of accuracy and computational time to take these partial derivatives analytically. Why then do we not proceed without any numerical differentiation?

In fact we do take partial derivatives analytically whenever possible. This allows for a faster, more accurate result. However, it is not always possible to take the partial derivative analytically; for example, when no closed analytic form exists. For these parameters, it is necessary to take partial derivatives numerically and to do so in a way that does not impact the model too severely.

Chapter 4

A phenomenological model for modified dispersion relations

4.1 Model framework

A schematic diagram of the model is provided in Fig 4.1 and the full code is available for download from `github.com/michellegurevich/gravitationalwaves`. We also provide an overview of the code structure and the main purpose of each file.

The code is organized in two directories:

- *cosmology* contains `jupyter` notebooks for
  - setting and plotting cosmological distances using `CAMB`
  - populating and plotting waveform examples of timeseries, frequency evolution, and demodulated signals using `PyCBC` waveforms
- *modgravity* contains
  - `main.py` file for running the program
  - `distances.py` file for calculating the standard luminosity distance D_L, modified luminosity distance D_α, and conformal distance term χ
  - `waveforms.py` file to calculate the phenomenological parameters $\vec{\theta} = (\alpha, \mathbb{A}, m_g, \zeta, \beta, \lambda_\mathbb{A})$; the standard and modified amplitudes A_S and A_M; the phase terms Ψ_S,

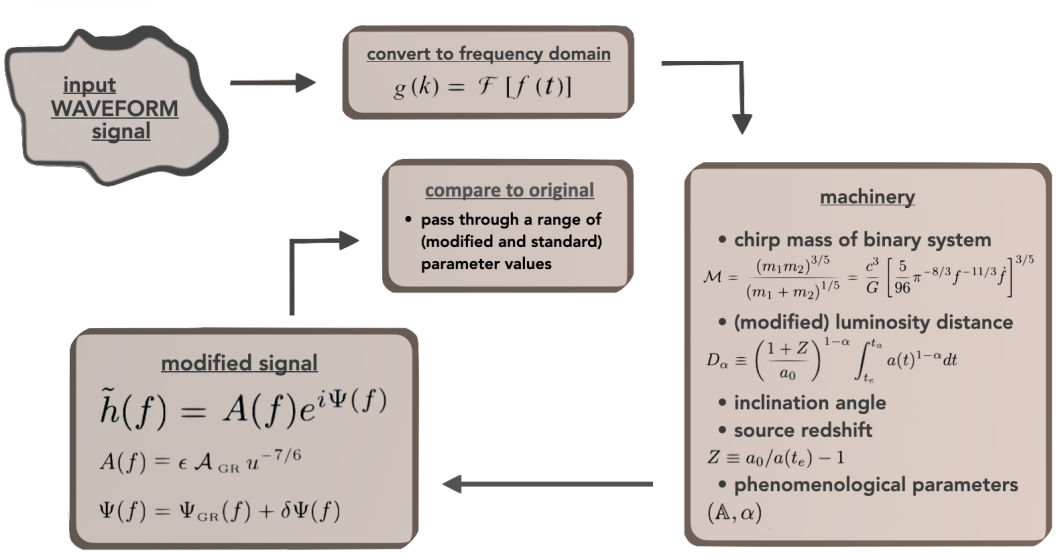

Figure 4.1: Schematic diagram of the model outlining its basic structure and expected inputs/outputs. The machinery consists of determining a set of cosmological parameters for the standard waveform $h(f)$ and then applying a set of phenomenological parameters $\vec{\theta}$ to produce a modified waveform $\tilde{h}(f)$. These are then compared to each other visually and statistically, using a Fisher analysis.

$\Psi_{\rm M}$, and $\delta\Psi$ (including numerical coefficients); any necessary constants such as v_{slo}, ϵ, or $\mathcal{M}$; the inner product decomposition described in Section 3.3.2

– `figures.py` file used for plotting many of the consistency checks; for example, plots of the Hubble parameter $H(t)$, the distance ratio D_α/D_L, the conformal factor ratio χ_M/χ_S, $h(f)$ and $\tilde{h}(f)$, and the phase behavior verification

– `fisher runs.ipynb` file to define a set of parameters (cosmological, phenomenological, and waveform), call the model to generate a modified signal using these parameters as input, pick a power spectrum density based on detector choice, and calculate the analytical derivatives for a Fisher matrix

– *tests* directory for verifying the integration with `PyCBC`, i.e. extending the library to include our standard and modified waveforms as `FrequencySeries` and `TimeSeries` objects

4.1.1 Analytical partial derivatives

The analytic derivatives ∂_i for the set of parameters $\vec{\theta}$ are calculated using the waveform expressions of Eq. (3.16) and (3.17) with $\beta = \zeta = 0$, and for a mass ratio,

$$\eta = \frac{m_1 m_2}{(m_1 + m_2)^2}$$

- $A_{\rm S}$, the standard amplitude: $\frac{\partial \tilde{h}(f)}{\partial \ln A_{\rm S}} = \tilde{h}(f)$
- $\Psi_{\rm S}$, the standard phase: $\frac{\partial \tilde{h}(f)}{\partial \Psi_{\rm S}} = -i\tilde{h}(f)$
- β, the non-linearity measure: $\frac{\partial \tilde{h}(f)}{\partial \beta} = -iu^{-1}\tilde{h}(f)$
- t_c, the fiducial time of emission: $\frac{\partial \tilde{h}(f)}{\partial f_0 t_c} = 2\pi i\,(f/f_0)\,\tilde{h}(f)$
- $\mathcal{M}$, the (observed) chirp mass:
  $\frac{\partial \tilde{h}(f)}{\partial \ln \mathcal{M}} = -\tilde{h}(f)\left(\frac{5i}{128}u^{-5/3} + \frac{5i}{96}\left(\frac{743}{336} + \frac{11\eta}{4}\right)\eta^{-2/5}u^{-1} - \frac{i\pi}{4}\eta^{-3/5}u^{-2/3}\right)$

Combinations of pairs of these partial derivatives correspond to entries in the Fisher matrix as described in Section 3.4.2. We note many of the partial derivatives have terms of $\tilde{h}(f)$ and recall the modified signal involves both + and × polarization components. Thus, we can finally express the Fisher matrix for our particular signal.

$$F_{ij} = \sum_{\boldsymbol{H}} \frac{\partial^2}{\partial\theta_i \partial\theta_j} \int_{f_{min}}^{f_{max}} \frac{|\boldsymbol{h}_f|^2}{|\boldsymbol{N}_f|^2} df \tag{4.1}$$

where $\boldsymbol{h}_f = h^+(f,\vec{\theta}) + h^\times(f,\vec{\theta})$ and $\boldsymbol{H}$ is the total population of signals. The polarization coordinates have implicitly been assumed, but should generally be $h_{ij} \sim \sum_p \int df d^3\Omega \epsilon_{ij} h^p(f)$. An extension of this model would consider general polarization coordinates as they have particular importance for determining which signals are being received. For example, those signals that approach longitudinally are not accounted for, and though their phase information would be impossible to reconstruct *a priori*, it is useful to describe exactly what proportion of total signals is captured.

4.2 Discussion and outlook

The direct detection in 2015 of gravitational waves from a binary black hole merger [3] a century after Albert Einstein first predicted their existence provided not only support for his theory of general relativity, but also the opportunity to probe the limits of that theory. As we enter the statistical era of gravitational wave research, exciting new instruments will allow us to take increasingly more accurate measurements of strong-gravity systems. The first direct detection of gravitational waves, **GW150194**, came from a black hole of mass $62M_{\odot}$ whose two components were originally $36M_{\odot}$ and $29M_{\odot}$, meaning the energy radiated out in gravitational waves was on the order of $3M_{\odot}c^2$ [3]. Since then, dozens more observations have been picked up by LIGO, and with multiple detectors slated for operation in coming decades, this number is expected to grow tremendously.

4.2.1 Future detectors: toward a complete picture of frequency

Detectors such as LISA, and ET will observe new frequency ranges and new classes of objects – opening gravitational wave cosmology to its multi-messenger era. These detectors will be able to detect signals from EMRIs, neutron star mergers, IMBHs, and individual black holes [6][44]. The overlap between those frequency bands and LIGO will also mean a network of detectors will be able to track a single strain as it passes through multiple frequencies.

LISA will look for gravitational wave signals in the mHZ band, and the ET will better constrain signals already picked up by LIGO. In addition to these inferometer-based detectors, observatories such as NanoGrav and other pulsar timing arrays (PTAs) will detect in the nHz frequency range [59]. The benefit of observing a different set of objects, in this case pulsars rather than black hole or neutron star mergers, is these may introduce new behaviors into the emitted gravitational waves not seen in current observations.

The launch of new facilities makes this an extremely exciting time to be involved in developing predictions, as it will be possible to verify or refine these as signals come in. For this reason, the phenomenological model developed here is designed to be sufficiently general so as to allow for application to new detectors.

4.2.2 Possible model extensions

It is worth noting there are several natural extensions to this project that benefit from its generalized design. In particular, we discuss here the possibility of admitting new polarization modes, incorporating higher-order geodesic perturbations, and making the model more widely accessible.

Separately, gravitational waves can possibly introduce new fundamental physics in describing polarization modes. Though general relativity admits two types of wave polarization, h_x and h_+, a strong stochastic cosmological gravitational wave background could be expected to contain up to six [60]. Because of its configuration for both frequency and angular modifications, and as a result of its multiple orbiter design, LISA could measure such a background [26]. The phenomenological model built here could be easily updated to incorporate such modes, and the machinery is already there to analyze how parameters would interact with them.

One consideration is to test for the graviton equivalent of the integrated Sachs-Wolfe effect, which describes how the cosmological redshifting of photons leads to uneveness in the cosmic microwave background radiation [41]. This effect has been studied for gravitational radiation using scalar perturbations to the FRW metric and shown to produce measurable changes to frequency among other parameters [61].

An extended model would ideally include a user interface allowing users to directly enter (ranges of) values for parameters that would then connect to the back-end, which would produce a modified waveform and an analysis of its behavior relative to GR. One drawback of the current software for generating waveforms is it requires users to install and run the libraries on their local machines, something which is not unusual by any means but which is susceptible to occasional breakdowns, e.g. maintaining redundant dependencies or overriding local environments. How could the project be abstracted and what would it look like as a 'complete' piece of machinery – for example, one that could be used by students interested in modifying waveforms phenomenologically themselves?

4.3 Conclusions

We have described the scientific context of modified gravity and gravitational wave dispersion, derived the theoretical foundations for such theories, and elaborated on the standard

and modified waveforms that are used to study extensions to GR. The main result of this project was to formulate and implement a phenomenological model to study frequency-dependent changes to gravitational waves. A secondary contribution was the derivation of several analytic partial derivatives and the corresponding Fisher matrix, which can be used to study correlations between the phenomenological and Lorentz-violating parameters and constrain data.

The outlook for gravitational wave cosmology is an exciting one, and we may well answer some of the questions posed here in coming years. It will be interesting to see what new questions those answers give rise to.

References

[1] Josu C. Aurrekoetxea, Pedro G. Ferreira, Katy Clough, Eugene A. Lim, and Oliver J. Tattersall. Where is the ringdown? Reconstructing quasinormal modes from dispersive waves, May 2022.

[2] B. P. Abbott et al. A guide to LIGO–Virgo detector noise and extraction of transient gravitational-wave signals. *Classical and Quantum Gravity*, 37(5):055002, March 2020.

[3] B. P. Abbott et al. Observation of Gravitational Waves from a Binary Black Hole Merger. *Physical Review Letters*, 116(6):061102, February 2016.

[4] Charles Misner, John Wheeler, and Kip Thorne. *Gravitation.* Freeman, 1973.

[5] Michael Rowan-Robinson. *Cosmology.* Oxford University Press, fourth edition, 2004.

[6] M. Bailes et al. Gravitational-wave physics and astronomy in the 2020s and 2030s. *Nature Reviews Physics*, 3(5):344–366, May 2021.

[7] Claudia de Rham and Gregory Gabadadze. Generalization of the Fierz-Pauli Action. *Physical Review D*, 82(4):044020, August 2010.

[8] Timothy Clifton, Pedro G. Ferreira, Antonio Padilla, and Constantinos Skordis. Modified Gravity and Cosmology. *Physics Reports*, 513(1-3):1–189, March 2012.

[9] Claudia de Rham. Massive Gravity. *Living Reviews in Relativity*, 17(1):7, December 2014.

[10] Chloe Gowling and Mark Hindmarsh. Observational prospects for phase transitions at LISA: Fisher matrix analysis. *Journal of Cosmology and Astroparticle Physics*, 2021(10):039, October 2021.

[11] A. Addazi et al. Quantum gravity phenomenology at the dawn of the multi-messenger era – A review. *Progress in Particle and Nuclear Physics*, 125:103948, July 2022.

[12] Claudia de Rham, Gregory Gabadadze, and Andrew J. Tolley. Resummation of Massive Gravity. *Physical Review Letters*, 106(23):231101, June 2011.

[13] G. Ashton, R. Prix, and D.I. Jones. A semicoherent glitch-robust continuous-gravitational-wave search method. *Physical Review D*, 98(6):063011, September 2018.

[14] Claudia de Rham and Scott Melville. Gravitational Rainbows: LIGO and Dark Energy at its Cutoff. *Physical Review Letters*, 121(22):221101, November 2018.

[15] T. Baker, E. Bellini, P.G. Ferreira, M. Lagos, J. Noller, and I. Sawicki. Strong Constraints on Cosmological Gravity from GW170817 and GRB 170817A. *Physical Review Letters*, 119(25):251301, December 2017.

[16] Tessa Baker, Gianluca Calcagni, Anson Chen, Matteo Fasiello, Lucas Lombriser, Katarina Martinovic, Mauro Pieroni, Mairi Sakellariadou, Gianmassimo Tasinato, Daniele Bertacca, and Ippocratis D. Saltas. Measuring the propagation speed of gravitational waves with LISA, March 2022.

[17] Nicolas Yunes, Kent Yagi, and Frans Pretorius. Theoretical Physics Implications of the Binary Black-Hole Mergers GW150914 and GW151226. *Physical Review D*, 94(8):084002, October 2016.

[18] M Göckeler and T Schücker. *Differential geometry, gauge theories, and gravity.* Cambridge University Press, first edition, 1987.

[19] Kurt Hinterbichler. Theoretical Aspects of Massive Gravity. *Reviews of Modern Physics*, 84(2):671–710, May 2012.

[20] Alexandre Le Tiec and Jérôme Novak. Theory of Gravitational Waves. pages 1–41. April 2017.

[21] Clifford M. Will. Bounding the mass of the graviton using gravitional-wave observations of inspiralling compact binaries. *Physical Review D*, 57(4):2061–2068, February 1998.

[22] Saeed Mirshekari, Nicolas Yunes, and Clifford M. Will. Constraining Lorentz-violating, Modified Dispersion Relations with Gravitational Waves. *Physical Review D*, 85(2):024041, January 2012.

[23] Drew Keppel and P. Ajith. Constraining the mass of the graviton using coalescing black-hole binaries. *Physical Review D*, 82(12):122001, December 2010.

[24] Gaetano Lambiase, Mairi Sakellariadou, and Antonio Stabile. Constraints on extended gravity models through gravitational wave emission. *Journal of Cosmology and Astroparticle Physics*, 2021(03):014, March 2021.

[25] Jose Maria Ezquiaga, Wayne Hu, Macarena Lagos, and Meng-Xiang Lin. Gravitational wave propagation beyond general relativity: waveform distortions and echoes. *Journal of Cosmology and Astroparticle Physics*, 2021(11):048, November 2021.

[26] Jeff Crowder and Neil J. Cornish. Beyond LISA: Exploring Future Gravitational Wave Missions. *Physical Review D*, 72(8):083005, October 2005.

[27] Michael L Katz and Shane L Larson. Evaluating black hole detectability with LISA. *Monthly Notices of the Royal Astronomical Society*, 483(3):3108–3118, March 2019.

[28] Nicola Bartolo, Daniele Bertacca, Robert Caldwell, Carlo R. Contaldi, Giulia Cusin, Valerio De Luca, Emanuela Dimastrogiovanni, Matteo Fasiello, Daniel G. Figueroa, Gabriele Franciolini, Alexander C. Jenkins, Marco Peloso, Mauro Pieroni, Arianna Renzini, Angelo Ricciardone, Antonio Riotto, Mairi Sakellariadou, Lorenzo Sorbo, Gianmassimo Tasinato, Jesus Torrado, Sebastien Clesse, and Sachiko Kuroyanagi. Probing Anisotropies of the Stochastic Gravitational Wave Background with LISA, January 2022.

[29] Alexandre Toubiana, Stanislav Babak, Enrico Barausse, and Luis Lehner. Modeling gravitational waves from exotic compact objects. *Physical Review D*, 103(6):064042, March 2021.

[30] Jillian Bellovary, Alyson Brooks, Monica Colpi, Michael Eracleous, Kelly Holley-Bockelmann, Ann Hornschemeier, Lucio Mayer, Priya Natarajan, Jacob Slutsky, and Michael Tremmel. Where are the Intermediate Mass Black Holes?, March 2019.

[31] LISA Technology: Interferometry explained, June 2020.

[32] Curt Cutler. Angular resolution of the LISA gravitational wave detector. *Physical Review D*, 57(12):7089–7102, June 1998.

[33] B. P. Abbott et al. Tests of General Relativity with the Binary Black Hole Signals from the LIGO-Virgo Catalog GWTC-1. *Physical Review D*, 100(10):104036, November 2019.

[34] P. Ajith. Gravitational-wave data analysis using binary black-hole waveforms. *Classical and Quantum Gravity*, 25(11):114033, June 2008.

[35] Alessandra Buonanno, Bala Iyer, Evan Ochsner, Yi Pan, and B. S. Sathyaprakash. Comparison of post-Newtonian templates for compact binary inspiral signals in gravitational-wave detectors. *Physical Review D*, 80(8):084043, October 2009.

[36] Yi Pan, Alessandra Buonanno, John G. Baker, Joan Centrella, Bernard J. Kelly, Sean T. McWilliams, Frans Pretorius, and James R. van Meter. A data-analysis driven comparison of analytic and numerical coalescing binary waveforms: nonspinning case. *Physical Review D*, 77(2):024014, January 2008.

[37] Clifford M. Will. On the unreasonable effectiveness of the post-Newtonian approximation in gravitational physics. *Proceedings of the National Academy of Sciences*, 108(15):5938–5945, April 2011.

[38] Patricia Schmidt. Gravitational Waves From Binary Black Hole Mergers: Modeling and Observations. *Frontiers in Astronomy and Space Sciences*, 7:28, June 2020.

[39] Hee-Suk Cho. Testing the validity of the phenomenological gravitational waveform models for nonspinning binary black hole searches at low masses. *Classical and Quantum Gravity*, 32(21):215023, November 2015.

[40] Serge Droz, Daniel J. Knapp, Eric Poisson, and Benjamin J. Owen. Gravitational waves from inspiraling compact binaries: Validity of the stationary-phase approximation to the Fourier transform. *Physical Review D*, 59(12):124016, May 1999.

[41] Scott Dodelson. *Modern Cosmology*. Academic Press, first edition, 2003.

[42] Enis Belgacem, Yves Dirian, Stefano Foffa, and Michele Maggiore. The gravitational-wave luminosity distance in modified gravity theories. *Physical Review D*, 97(10):104066, May 2018.

[43] Saeed Mirshekari. Gravitational Waves and Inspiraling Compact Binaries in Alternative Theories of Gravity. page 238.

[44] Shu-Cheng Yang, Wen-Biao Han, Shuo Xin, and Chen Zhang. Testing dispersion of gravitational waves from eccentric extreme-mass-ratio inspirals. *International Journal of Modern Physics D*, 28(15):1950166, November 2019.

[45] Anders Brandt and Rune Brincker. Integrating time signals in frequency domain – Comparison with time domain integration. *Measurement*, 58:511–519, December 2014.

[46] A. F. Ferrari and A. Yu Petrov. Lorentz violation in the linearized gravity. In *CPT and Lorentz Symmetry*, pages 267–270, December 2010.

[47] Matthew Mewes. Signals for Lorentz violation in gravitational waves. *Physical Review D*, 99(10):104062, May 2019.

[48] S. Mastrogiovanni, D. Steer, and M. Barsuglia. Probing modified gravity theories and cosmology using gravitational-waves and associated electromagnetic counterparts. *Physical Review D*, 102(4):044009, August 2020.

[49] David Alonso, Carlo R. Contaldi, Giulia Cusin, Pedro G. Ferreira, and Arianna I. Renzini. Noise angular power spectrum of gravitational wave background experiments. *Physical Review D*, 101(12):124048, June 2020.

[50] Tristan L. Smith and Robert R. Caldwell. LISA for cosmologists: Calculating the signal-to-noise ratio for stochastic and deterministic sources. *Physical Review D*, 100(10):104055, November 2019.

[51] Christopher J. Moore, Robert H. Cole, and Christopher P. L. Berry. Gravitational-wave sensitivity curves. *Classical and Quantum Gravity*, 32(1):015014, January 2015.

[52] Eric Thrane and Joseph D. Romano. Sensitivity curves for searches for gravitational-wave backgrounds. *Physical Review D*, 88(12):124032, December 2013.

[53] Chandra Kant Mishra, K. G. Arun, Bala R. Iyer, and B. S. Sathyaprakash. Parametrized tests of post-Newtonian theory using Advanced LIGO and Einstein Telescope. *Physical Review D*, 82(6):064010, September 2010.

[54] A. F. Heavens, T. D. Kitching, and L. Verde. On model selection forecasting, Dark Energy and modified gravity. *Monthly Notices of the Royal Astronomical Society*, 380(3):1029–1035, August 2007.

[55] Arianna I. Renzini, Joseph D. Romano, Carlo R. Contaldi, and Neil J. Cornish. Comparison of maximum likelihood mapping methods for gravitational-wave backgrounds. *Physical Review D*, 105(2):023519, January 2022.

[56] Alan Heavens. Generalisations of Fisher Matrices. *Entropy*, 18(6):236, June 2016.

[57] Max Tegmark, Andy N. Taylor, and Alan F. Heavens. Karhunen-Loeve Eigenvalue Problems in Cosmology: How Should We Tackle Large Data Sets? *The Astrophysical Journal*, 480(1):22–35, May 1997.

[58] Michele Vallisneri. Use and Abuse of the Fisher Information Matrix in the Assessment of Gravitational-Wave Parameter-Estimation Prospects. *Physical Review D*, 77(4):042001, February 2008.

[59] George Hobbs and Shi Dai. Gravitational wave research using pulsar timing arrays. *National Science Review*, 4(5):707–717, September 2017.

[60] Sourav Roy Chowdhury and Maxim Khlopov. Gravitational waves in the modified gravity, November 2021.

[61] Pablo Laguna, Shane L. Larson, David Spergel, and Nicolas Yunes. Integrated Sachs-Wolfe Effect for Gravitational Radiation. *The Astrophysical Journal*, 715(1):L12–L15, May 2010.